ELECTROMAGNETIC ION CYCLOTRON INSTABILITY IN SPACE PLASMAS

M. N. S. Qureshi*, S. T. Rizwan and I. Ahmed

Department of Physics, GC University, Lahore 54000, Pakistan
*Corresponding Author: M. N. S. Qureshi
E-mail: noumansarwar@gcu.edu.pk

ABSTRACT: This study presents observations of ion waves having low-frequencies and their associated ion velocity distribution functions (VDFs) from the Earth's magnetosphere and solar wind, using the data from Cluster mission. The ion VDFs observed are characterized as non-Maxwellian, comprising a predominant cold component alongside hot tenuous components. We derive the dispersion relation of low-frequency ion waves, by fitting the parameters of observed VDFs, and numerically obtained the instability growth rate. We further investigate the influence of superthermal particles on the instability.

Keywords: EMIC waves; Ion distribution function; Non-Maxwellian distributions.

(Received 15.09.2024 Accepted 03.12.2024)

INTRODUCTION

The dynamics of space plasmas are primarily influenced by collective cyclotron wave-particle interactions. Previous researches (Xiao *et al*., 1998, 2006a; Lu and Wang, 2006; Lu *et al*., 2006), has shown that particle anisotropy often triggers instabilities in space plasmas, while increased particle scattering tends to diminish this anisotropy, leading to a stable state that aligns with an instability threshold. The foundational work by Kennel and Petschek (1966) has shown that particle distributions remain close to these instability thresholds due to wave-particle interaction caused by larger fluctuations, hence reducing the anisotropy. Previous investigations on bi-Maxwellian plasmas have shown that the threshold condition of electromagnetic ion cyclotron (EMIC) instability limits the temperature anisotropy of particles. This upper limit is inversely related to the particle parallel beta (Gary, 1993; Gary and Lee, 1994; Gary *et al*., 1994a, 1997). Observational analyses have confirmed this upper bound on superthermal proton temperature anisotropies in regions such as the magnetosheath, near geostationary orbit, and within the magnetosphere (Gary *et al*., 1993; Anderson *et al*., 1994; Fuselier *et al*., 1994).

According to the data observed by WIND/SWE, further investigations have shown that similar limitations on temperature anisotropy of protons by HELIOS observations (Marsch *et al*., 2004) and within solar wind plasma (Gary *et al*., 2001; Kasper *et al*., 2002, 2003, 2006). To explore the characteristics of anisotropy restrictions related to whistler instability, electron mirror instability, and electron Weibel instability, Gary and Karimabadi (2006) applied the linear theory. According to the observations, outer magnetosphere (L>5) is the region where ions particularly protons often consist of both the components, i.e., superthermal anisotropic and cold (Gurnett and Frank, 1974; McComas *et al*., 1993).

However, natural space plasmas are generally considered to be hot, tenuous, and collision-free, exhibit a clear non-Maxwellian tail in the profile of the distribution and effectively modelled by kappa distribution (Vasyliunas, 1968; Christon *et al*., 1988; Maksimovic *et al*., 1997; Viñas *et al*., 2005). Such population of enhanced tail is significantly affect the anisotropy instability threshold conditions linked, as velocity distribution plays a crucial role in determining particle anisotropy. It has been found that velocities significantly exceeding thermal speeds are primarily responsible for gyro-resonant wave-particle interactions. Xiao *et al*. (2006b) conducted a research on the whistler instability threshold condition, generally modelled using the bi-kappa distribution function, in regions where both hot anisotropic electron and cold plasma components are there. This research based on earlier studies focused on a single hot electron within a simple Maxwellian plasma (Gary and Wang, 1996; Gary *et al*., 2000, 2005).

Consequently, it is essential to employ an observed VDF for superthermal protons in a multi-species plasma to gain deeper understanding of the EMIC instability by deriving real frequency and growth rates. In Section 2, we present the observed distribution using Cluster data and fit it with the bi-Kappa distribution. We then employ the observed plasma parameters and the spectral index kappa to numerically calculate the real frequency and growth rate values.

Observed Distribution and Fitting: We use the following kappa distribution to model the observed distribution.

$$f_{\kappa\sigma} = \frac{1}{\pi^{\frac{3}{2}}\theta_{\perp}^{2}\theta_{\parallel}\kappa^{\frac{3}{2}}}\frac{\Gamma(\kappa+1)}{\Gamma(\kappa-\frac{1}{2})}\left[1+\frac{v_{\parallel}^{2}}{\kappa\theta_{\parallel}^{2}}+\frac{v_{\perp}^{2}}{\kappa\theta_{\perp}^{2}}\right]^{-(\kappa+1)} \quad (1)$$

where

$$\theta_{\parallel} = \sqrt{\frac{(2\kappa - 3)}{\kappa}}\sqrt{\frac{T_{\parallel}}{m}} \quad (2)$$

$$\theta_{\perp} = \sqrt{\frac{(2\kappa - 3)}{\kappa}}\sqrt{\frac{T_{\perp}}{m}} \quad (3)$$

are the parallel and perpendicular thermal speeds, respectively, modified due to the presence of κ. Here, Γ is gamma function, $m$be the ion mass, $T_{\parallel}$, $T_{\perp}$corresponds to the parallel and perpendicular temperatures, respectively, and $\sigma(= c, s, h)$ where c = cold, s = strahl, and h =hot.

We present in situ observation of Cluster C1 satellite on 18 July 2005, when it crosses the plasmaspheric plume. It is observed by Cluster C1 that EMIC waves scatter the RC ions in the outer boundary of plasmaspheric plume. We choose a time period when the EMIC waves excited and observed the ion velocity distribution at the time when the EMIC waves excitation is at the peak. In Fig. 1, the observed distribution is shown (blue solid circles) which is modelled by the bi-kappa distribution (red solid line). We can see that the observed distribution consists of three components cold, strhal and hot, and is well modelled by kappa distribution. The values of kappa indices and other observed parameters are shown in the figure caption that are used to model the observed distribution.

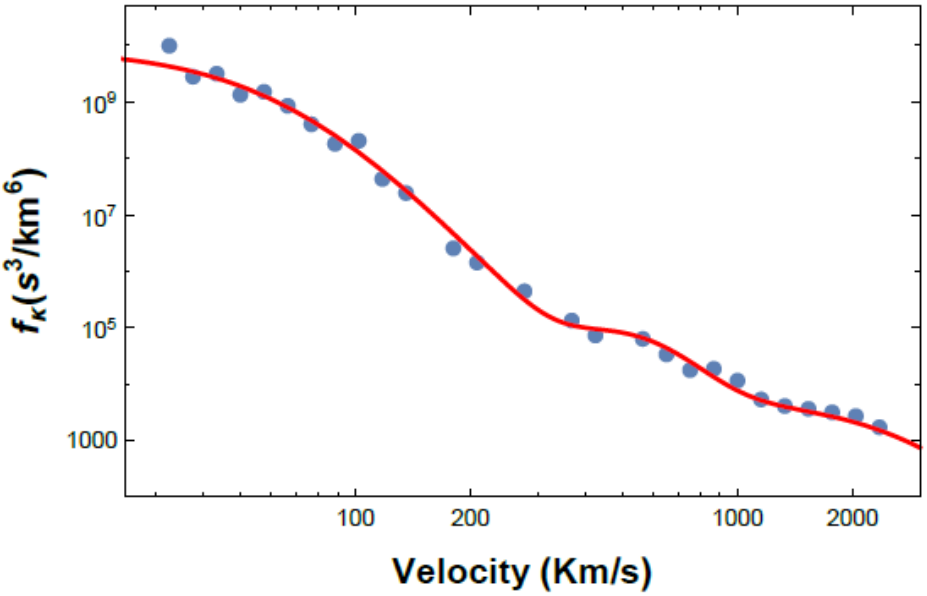

Figure 1: Fitting of the observed distribution with the kappa distribution. The fitting values are $\kappa_c = 2.7$, $\kappa_s = 1.8$, $\kappa_h = 15.1$, $n_c = 0.99922\, n$, $n_s = 0.00009\, n$, $n_h = 0.00069\, n$, $T_{c||} = 4.73974\, eV$, $T_{c\perp} = 18.959\, eV$, $T_{s||} = 51.7063\, eV$, $T_{s\perp} = 137.883\, eV$, $T_{h||} = 779.903\, eV$, $T_{h\perp} = 869.528\, eV$.

Real Frequency and Growth Rate: The general dispersion relation for electromagnetic hot plasma for the kappa distributed plasma in the parallel direction, is

$$\begin{vmatrix} \epsilon_{xx} - {n_{\parallel}}^2 & \epsilon_{xy} & \epsilon_{xz} + n_{\parallel}n_{\perp} \\ -\epsilon_{yx} & \epsilon_{yy} - n^2 & \epsilon_{yz} \\ -\epsilon_{zy} + n_{\parallel}n_{\perp} & -\epsilon_{zy} & \epsilon_{zz} - {n_{\perp}}^2 \end{vmatrix} = 0 \quad (4)$$

The trivial solution of equation (4) can be written as

$$\begin{vmatrix} \epsilon_{xx} - {n_{\parallel}}^2 & \epsilon_{xy} & \epsilon_{xz} + n_{\parallel}n_{\perp} \\ -\epsilon_{yx} & \epsilon_{yy} - n^2 & \epsilon_{yz} \\ -\epsilon_{zy} + n_{\parallel}n_{\perp} & -\epsilon_{zy} & \epsilon_{zz} - {n_{\perp}}^2 \end{vmatrix} = 0 \quad (5)$$

For parallel propagating waves $k_{\perp} = 0$, the above equation can be reduced as

$$\begin{vmatrix} \epsilon_{xx} - {n_\parallel}^2 & \epsilon_{xy} & 0 \\ \epsilon_{xy} & \epsilon_{xx} - {n_\parallel}^2 & 0 \\ 0 & 0 & \epsilon_{zz} \end{vmatrix} = 0 \tag{6}$$

We now solve the above determinant, as

$$(\epsilon_{xx} + i\epsilon_{xy} - \frac{c^2k^2}{\omega^2}) \cdot (\epsilon_{xx} - i\epsilon_{xy} - \frac{c^2k^2}{\omega^2}) = 0 \tag{7}$$

As, we know that the ϵ_{xy} and ϵ_{xy} components of hot dielectric tensor are (Summer *et al*., 1994)

$$\epsilon_{xy} = -\frac{i\,{\omega_{pi}}^2}{\omega^2}\frac{\omega}{\Omega_i} + i\frac{{\omega_{pi}}^2}{\omega^2}\left[\xi_0 Z_\kappa(\xi) + \left(1 + \xi Z_\kappa(\xi)\right)\left(\frac{\theta_\perp^2}{{\theta_\parallel}^2} - 1\right)\right] \tag{8}$$

$$\epsilon_{xx} = \frac{{\omega_{pi}}^2}{\omega^2}\left[\xi_0 Z_\kappa(\xi) + \left(1 + \xi Z_\kappa(\xi)\right)\left(\frac{\theta_\perp^2}{{\theta_\parallel}^2} - 1\right)\right] \tag{9}$$

Now by putting Eqs. (8) and (9) in Eq. (7), we get

$$\frac{c^2k^2}{{\omega_{pi}}^2} + \frac{\omega}{\Omega_i} - \left[\xi_0 Z_\kappa(\xi) + \left(\frac{\theta_\perp^2}{{\theta_\parallel}^2} - 1\right)\left(1 + \xi Z_\kappa(\xi)\right)\right] = 0 \tag{10}$$

where $\xi_0 = \frac{\omega}{k_\parallel \theta_\parallel}$, $\xi = \frac{\omega - \Omega}{k_\parallel \theta_\parallel}$ and

$$Z_\kappa(\xi) = \frac{1}{\sqrt{\pi}}\frac{\Gamma(\kappa+1)}{\Gamma(\kappa - 1/2)\kappa^{3/2}}\int_{-\infty}^{\infty}\frac{(1 + x^2/\kappa)^{-(\kappa+1)}}{(x - \xi)}dx \tag{11}$$

The above Eq. (10) is the dispersion relation of EMIC waves.

Numerical Results: In order to numerically plot the above dispersion relation, we write Eq. (10), as

$$0 = k^2 + z - \left[A_T + \frac{(A_T + 1)z - A_T}{k\left(1 - \frac{3}{2\kappa}\right)^{\frac{1}{2}}\beta_\parallel^{\frac{1}{2}}} Z\left(\frac{z - 1}{k\left(1 - \frac{3}{2\kappa}\right)^{\frac{1}{2}}\beta_\parallel^{\frac{1}{2}}}\right)\right] \tag{12}$$

where

$$z = \frac{\omega}{\Omega_i}\ ;\ k = \frac{ck}{\omega_{pi}}\ ;\ A_T = \frac{\theta_\perp^2}{{\theta_\parallel}^2} - 1 \text{ and } \beta_\parallel = \frac{8\,\pi\, n_0 T_\parallel}{B^2}.$$

In the above Eq. (12), we have taken $k_\parallel = k$. We now solve the Eq. (12) numerically and plot the real frequency and growth rate in Figs. 2 and 3 using the same parameters as given in Fig. 1. Figure 2 displays the real frequency of EMIC waves for kappa distributed plasma (solid black line) and for Maxwellian plasma (dashed black line). We note that real frequency for both the plasmas shows very similar behavior and there is not much difference between their values for all the range of wave numbers. Figure 3 displays the growth rates for kappa distributed plasma (solid blue line) as well as for Maxwellian plasma (dashed blue line). We note that the growth rate for kappa distributed plasma is not only higher than the Maxwellian plasma but also has a wide wavelength range.

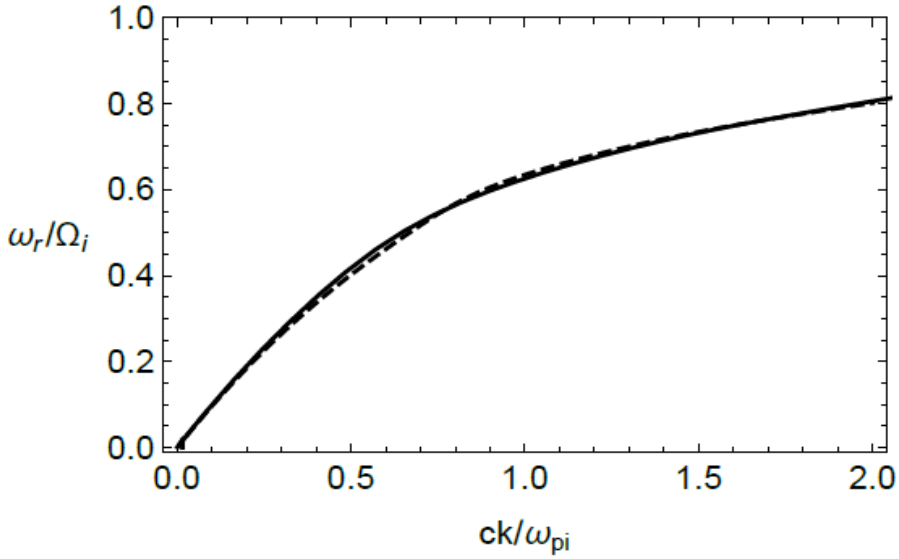

Figure 2: Real frequency for kappa distributed plasma (solid black line) and for Maxwellian plasma (dashed black line) for the same parameters given in Fig. 1.

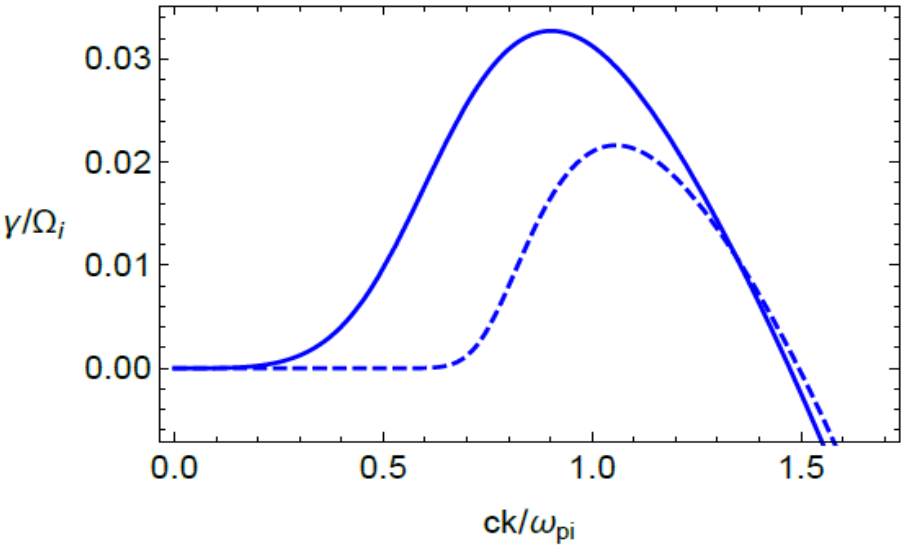

Figure 3: Growth rate for kappa distributed plasma (solid blue line) and for Maxwellian plasma (dashed blue line) for the same parameters given in Fig. 1.

Conclusion: This study presents the observations of ion VDF from the Earth's plasmaspheric plume using the Cluster 1 data when the EMIC waves are generated during the recovery phase of the geomagnetic storm that occurred on July 18, 2005. We observe the ion VDF when the EMIC wave activity is at its maximum. We found that the distribution contains three components, cold, strahl and hot. All these three components are modelled by using the bi-kappa distribution functions. Using the fitted values of kappa indices and corresponding observed parameters such as density and temperature, we plot the real frequency and growth rate plots for the EMIC waves. We found that the real frequency sows very little deviation from the Maxwellian, however, the growth rate is higher than the Maxwellian. We conclude that the growth rate observed from the Maxwellian underestimates the actual growth rate which is based on the observed distribution. Thus, we should use the observed values rather than rely on the idealized conditions as we have been doing in the past.

REFERENCES

Anderson, B. J., S. A. Fuselier, S. P. Gary and R. E. Denton, (1994). Magnetic spectral signatures in the Earth's magnetosheath and plasma depletion layer. *J. Geophys. Res.* 99, 5877.

Christon, S. P., D. G. Mitchell, D. J. Williams, L. A.

Frank, C. Y. Huang and T. E. Eastman, (1988). Energy spectra of plasmasheet ions and electrons from 50 eV/e to 1 MeV during plasma temperature transitions. *J. Geophys. Res.* 93, 2562.

Fuselier, S. A., B. J. Anderson, S. P. Gary and R. E. Denton, (1994) Inverse correlations between the ion temperature anisotropy and plasma beta in the Earth's quasi-parallel magnetosheath. *J. Geophys. Res.* 99, 14,931.

Gary, S. P., (1993). Theory of Space Plasma Microinstabilities. *Cambridge Univ. Press, New York.*

Gary, S. P., B. J. Anderson, R. E. Denton, S. A. Fuselier, M. E. McKean and D. Winske, (1993). Ion anisotropies in the magnetosheath. *Geophys. Res. Lett*. 20, 1767.

Gary, S. P., and M. A. Lee, (1994). The ion cyclotron anisotropy instability and the inverse correlation between proton anisotropy and proton beta. *J. Geophys. Res.* 99, 11,297.

Gary, S. P., M. E. McKean, D. Winske, B. J. Anderson, R. E. Denton and S. A. Fuselier, (1994a). The proton cyclotron instability and the anisotropy/ b inverse correlation. *J. Geophys. Res*. 99, 5903.

Gary, S. P. and J. Wang, (1996). Whistler instability: Electron anisotropy upper bound. *J. Geophys. Res.* 101, 10,749.

Gary, S. P., J. Wang, D. Winske and S. A. Fuselier, (1997). Proton temperature anisotropy upper bound. *J. Geophys. Res.* 102, 27,159.

Gary, S. P., D. Winske and M. Hesse, (2000). Electron temperature anisotropy instabilities: Computer simulations. *J. Geophys. Res.* 105, 10,751.

Gary, S. P., R. M. Skoug, J. T. Steinberg and C. W. Smith, (2001). Proton temperature anisotropy constraint in the solar wind: ACE observations. *Geophys. Res. Lett.* 28, 2759.

Gary, S. P., B. Lavraud, M. F. Thomsen, B. Lefebvre and S. J. Schwartz, (2005). Electron anisotropy constraint in the magnetosheath: Cluster observations. *J. Geophys. Res.* 32, L13109.

Gary, S. P. and H. Karimabadi, (2006). Linear theory of electron temperature anisotropy instabilities: Whistler, mirror, and Weibel. *J. Geophys. Res.* 111, A11224.

Gurnett, D. A. and L. A. Frank, (1974). Thermal and suprathermal plasma densities in the outer magnetosphere. *J. Geophys. Res.* 79, 2355.

Kasper, J. C., A. J. Lazarus and S. P. Gary, (2002). Wind/SWE observations of firehose constraint on solar wind proton temperature anisotropy. *Geophys. Res. Lett.* 29(17), 1839.

Kasper, J. C., A. J. Lazarus, S. P. Gary and A. Szabo, (2003). Solar wind temperature anisotropies. *Solar Wind Ten*, edited by Velli, M., Bruno, R., and Malara, F. *AIP Conf. Proc*. 679, 538– 541.

Kasper, J., A. J. Lazarus, J. T. Steinberg, K. W. Ogilvie and A. Szabo, (2006). Physics-based tests to identify the accuracy of solar wind ion measurements: A case study with the Wind Faraday cups. *J. Geophys. Res.* 111, A03105.

Kennel, C. F., and H. E. Petschek, (1966). Limit on stably trapped particle fluxes. *J. Geophys. Res.* 71, 1.

Lu, Q. M., and S. Wang, (2006). Electromagnetic waves downstream of quasi-perpendicular shocks. *J. Geophys. Res.* 111, A05204.

Lu, Q. M., F. Guo and S. Wang, (2006). Magnetic spectral signatures in the terrestrial plasma depletion layer: Hybrid simulations. *J. Geophys. Res.* 111, A04207.

Maksimovic, M., V. Pierrard and J. F. Lemaire, (1997). A kinetic model of the solar wind with Kappa distribution functions in the corona. *Astron. Astrophys.* 324, 725.

Marsch, E., X. Z. Ao and C. Y. Tu, (2004). On the temperature anisotropy of the core part of the proton velocity distribution function in the solar wind. *J. Geophys. Res.* 109, A04102.

McComas, D. J., S. J. Blame, B. L. Barraclough, J. R. Donart, R. C. Elphic, J. T. Gosling, M. B. Moldwin, K. R. Moore and M. F. Thomsen, (1993). Magnetoshperic plasma analyzer: Initial three-spacecraft observations from geosynchronous orbit. *J. Geophys. Res.* 98, 13,453.

Summer, D., S. Xue and R. M. Thorne, (1994). Calculation of the dielectric tensor for a generalized (kappa) distribution function. *Phys. Plasmas.* 1, 2012.

Vasyliunas, V. M., (1968). A survey of low-energy electrons in the evening sector of the magnetosphere with OGO 1 and OGO 3. *J. Geophys. Res.* 73, 2839.

Vin˜as, A. F., R. L. Mace and R. F. Benson, (2005). Dispersion characteristics for plasma resonances of Maxwellian and Kappa distribution plasmas and their comparisons to the IMAGE/RPI observations. *J. Geophys. Res.* 110, A06202.

Xiao, F., R. M. Thorne and D. Summers, (1998). Instability of electromagnetic R-mode waves in a relativistic plasma. *Phys. Plasmas*. 5, 2489.

Xiao, F., Q. Zhou, H. He and L. Tang, (2006a). Instability of whistler-mode waves by a relativistic kappa-loss-cone distribution in space plasmas. *Plasma Phys. Controlled Fusion.* 48, 203.

Xiao, F., Q. Zhou, H. Zheng and S. Wang, (2006b). Whistler instability threshold condition of energetic electrons by kappa distribution in space plasmas. *J. Geophys. Res.* 111, A08208.